# Liquefaction Constitutive Model

**Proc. Intl. Workshop on The Physics and Mechanics of Soil Liquefaction, Lade, P., Ed., Sept. 10-11, Baltimore, MD, Balkema, 1998.**

Ahmed-W. Elgamal
*Univ. of California, San Diego, La Jolla, CA-USA 92093*

Ender Parra
*INTEVEP, SA, Venezuela*

Zhaohui Yang
*Columbia University, NY, NY-USA 10027*

Ricardo Dobry
*Rensselaer Polytechnic Institute, Troy, NY-USA 12180*

Mourad Zeghal
*Rensselaer Polytechnic Institute, Troy, NY-USA 12180*

ABSTRACT: A constitutive model is developed to reproduce salient aspects associated with seismically-induced soil liquefaction. Attention is mainly focused on the deviatoric (shear) stress-strain response mechanism. Soil shear behavior during liquefaction is modeled to display a significant regain in stiffness and strength with the increase in deformation during each cycle of applied load. This behavior appears to play a major role in dictating the magnitude of shear deformations as observed in laboratory tests and manifested in acceleration records from earthquakes and centrifuge experiments.

KEYWORDS: Liquefaction, cyclic-mobility, sand, soil, constitutive modeling, earthquake, plasticity

## 1. INTRODUCTION

During liquefaction, recent records (Holzer *et al.* [16]) of seismic site response have manifested a possible strong influence of soil dilation during cyclic loading. Such phases of dilation may result in significant regain in shear stiffness and strength at large cyclic shear strain excursions, leading to: i) associated instances of pore-pressure reduction, ii) appearance of spikes in lateral acceleration records (as a direct consequence of the increased shear resistance), and most importantly, iii) a strong restraining effect on the magnitude of cyclic and accumulated permanent shear strains. This restraint on shear strain has been referred

to as a form of cyclic-mobility in a large number of pioneering liquefaction studies (*e.g.,* Seed and Lee [26], Casagrande [4], Castro [5], Castro and Poulos [6], Seed [27]). For the important situations of biased strain accumulation due to an initial locked-in shear stress, this pattern of behavior may play a dominant role in dictating the extent of such deformations. Currently, the above mentioned effects are also thoroughly documented by a large body of experimental research (employing clean sands and clean non-plastic silts), including centrifuge experiments (*e.g.,* Dobry *et al.* [9], Taboada [28], Dobry *et al.* [10]), shake-table tests, and cyclic laboratory sample tests (Arulmoli [1]). A thorough summary is provided (Elgamal *et al.* [14]) of the relevant: i) seismic response case histories, ii) recorded experimental (centrifuge, shake table and laboratory) response, and iii) constitutive models developed to address this phenomenon.

In the following pages, illustrations of the above-described shear stress-strain mechanisms are presented. Thereafter, the constitutive model is discussed along with an appropriate finite element computational framework. Finally, the salient model response characteristics are displayed.

## 2. CYCLIC LOADING DURING LIQUEFACTION

A thorough review of available literature has been presented recently by Elgamal *et al.* [14]. An illustration of the mechanisms observed in undrained cyclic laboratory tests is shown in Figures 1 and 2 (Arulmoli *et al.* [1]). Similar response (Figures 3 - 5) was observed (Holzer *et al.* [16], Youd and Holzer [31], Zeghal and Elgamal [32]) at the US Imperial County Wildlife Refuge site (1987 Superstition Hills earthquake records). One-dimensional shear stress-strain histories (Figure 6) calculated from recorded centrifuge experiment acceleration and LVDT records (Dobry *et al.* [9], Dobry *et al.* [10], Taboada [28], Elgamal *et al.* [13]) also display a similar response mechanism. Figures 2 and 6 depict the mechanism of accumulation of cycle-by-cycle deformations. Accuracy in reproducing this mechanism is among the most important goals of the developed constitutive model.

## 3. THEORETICAL BASIS

The model framework follows the procedures developed by Prevost [24], based on the multiple yield surface plasticity concept (Iwan [19], and Mroz [22]). It was modified (Parra [23]) from its original form (Prevost [24]) to model the shear stress-strain features discussed above (Figs. 1 - 6). Special attention was given to the deviatoric – volumetric strain coupling under cyclic loading; in particular during loading – unloading – reloading above the phase transformation line.

Following the usual cyclic soil plasticity concepts (*e.g.,* Prevost [24]), a strain increment $\dot{\boldsymbol{\epsilon}}$ is assumed to be the sum of elastic and plastic strain increments, denoted $\dot{\boldsymbol{\epsilon}}^e$ and $\dot{\boldsymbol{\epsilon}}^p$ respectively. The material elasticity is linear and isotropic, and nonlinearity and anisotropy result from plasticity. In order to describe the material's plasticity one needs [24]: *a)* the yield condition specifying the states of stress for which plastic flow occurs; *b)* the flow rule relating the plastic strain increment tensor to the stress and stress increment tensors; and *c)* the hardening rule specifying yield condition

modification in the course of plastic flow. In the following sections, stress and strain are assumed positive in tension and negative in compression. All normal stresses are effective, so that drained, partially drained and undrained situations may be analyzed using the same framework. Currently available constitutive models that reproduce important aspects of above shear mechanism include those by Iai [17, 18] and Tateishi *et al.* [29].

### 3.1 *Constitutive Equations*

The constitutive equation is written in incremental form as follows (Prevost [24]):

$$\dot{\boldsymbol{\sigma}} = \mathbf{E} : ( \dot{\boldsymbol{\epsilon}} - \dot{\boldsymbol{\epsilon}}^p) \tag{1}$$

where

$\dot{\boldsymbol{\sigma}}$ = rate of effective Cauchy stress tensor
$\dot{\boldsymbol{\epsilon}}$ = rate of deformation tensor
$\dot{\boldsymbol{\epsilon}}^p$ = plastic rate of deformation tensor
$\mathbf{E}$ = isotropic elastic coefficient tensor

The plastic rate of deformation tensor is defined by [15, 24]:

$$\dot{\boldsymbol{\epsilon}}^p = \mathbf{P} \ \langle L \rangle \tag{2}$$

where $\mathbf{P}$ is a symmetric second-order tensor that defines the direction of plastic deformation in stress space, $L$ is the plastic loading function, and the symbol $\langle \ \ \rangle$ denotes the MacCauley's brackets, *viz.*,

$$\langle L \rangle = \begin{cases} L & \text{if } L > 0 \\ 0 & \text{otherwise} \end{cases} \tag{3}$$

The function $L$ is defined by [15]:

$$L = \frac{1}{H'} \mathbf{Q} : \dot{\boldsymbol{\sigma}} \tag{4}$$

where $\mathbf{Q}$ is a symmetric second-order tensor that defines direction of outer normal to the yield surface, and $H'$ is the plastic modulus. It is convenient to decompose $\mathbf{P}$ and $\mathbf{Q}$ into their deviatoric and volumetric components [24] such that:

$$\mathbf{P} = \mathbf{P}' + P'' \, \boldsymbol{\delta} \tag{5}$$
$$\mathbf{Q} = \mathbf{Q}' + Q'' \, \boldsymbol{\delta} \tag{6}$$

where $\boldsymbol{\delta}$ is the second-order identity tensor.

Combining Eqs. 1 and 2, Eq. 4 can be rewritten as

$$L = \frac{1}{H' + H_0} \mathbf{Q} : \mathbf{E} : \dot{\boldsymbol{\sigma}} \tag{7}$$

where

$$H_0 = \mathbf{Q} : \mathbf{E} : \mathbf{P} = B \ (3P'') \ (3Q'') + 2\,G\,\mathbf{P}' : \mathbf{Q}' \tag{8}$$

### 3.2 *Yield Function*

The yield function (Fig. 7) that represents the states of stress for which plastic flow occurs, is selected of the following form [21, 24]:

$$f = \frac{3}{2} ( \boldsymbol{s} - p_a \boldsymbol{\alpha}) : ( \boldsymbol{s} - p_a \boldsymbol{\alpha}) - \ m^2 p_a^2 = 0 \tag{9}$$

where

$\boldsymbol{s} = \boldsymbol{\sigma} - p \, \boldsymbol{\delta}$ = deviatoric stress tensor
$\boldsymbol{\sigma}$ = effective Cauchy stress tensor (negative in compression)
$p_a = p - a$
$p = \frac{1}{3} tr ( \boldsymbol{\sigma} )$ = effective mean normal stress
$a$ = material constant ( $a = c / \tan \phi$ where $c$ = cohesion and $\phi$ = friction angle )
$\boldsymbol{\alpha}$ = kinematic deviatoric tensor defining the coordinates of the yield surface center in deviatoric stress subspace
$M$ = material parameter related to the friction angle $\phi$

The adopted yield function, plotted in stress space forms a conical surface with its apex at "$a$" along the hydrostatic axis as shown in Figs. 5, 7 and 8. For cohesionless soils, $a$ may be viewed as a low shear strength associated with the condition ($p = 0$).

The initial position of a yield surface given by $\boldsymbol{\alpha}$, reflects the degree of material or stress induced anisotropy, and it is considered as the material's memory of its fabric or past loading history. If $\boldsymbol{\alpha} = \mathbf{0}$, the axis of the cone coincides with the space diagonal, and the model will result in an initially isotropic behavior. Neglecting the influence of the Lode angle in the definition of $M$ allows any deviatoric plane ($p$ = constant) to intersect a circular cross-section of the yield surface. The center of this plane does not generally coincide with the space diagonal, but is shifted by the amount $p_a\boldsymbol{\alpha}$ in principal stress space (Fig. 7) .

The outer normal to the yield surface, $\mathbf{Q}$, may be normalized in any convenient fashion, and in the following:

$$\mathbf{Q} : \mathbf{Q} = \mathbf{Q}' : \mathbf{Q}' + \frac{1}{3}\,(3Q'')^2 = 1 \qquad (10)$$

### 3.3 *Flow Rule*

In order to characterize the volume change effects correctly, it is necessary to employ a non-associated flow rule [2, 8, 24]. Typically, non-associativity is restricted to the dilatational component of the plastic flow in accordance with experimental observations of granular material response [2, 24].

A distinction between these main volumetric response mechanisms is made, so that the flow rule is defined separately for stress states above, on, or below the phase transformation line (Fig. 8) using a phenomenological approach. Thus, the flow rule is given by:

$$\mathbf{P}' = \mathbf{Q}' \qquad \text{(associated)} \qquad (11)$$

$$3P'' = \chi(\eta, \eta_{pt}, p, a, \xi^p) \qquad \text{(non-associated)} \qquad (12)$$

where $\eta = \left(\frac{3}{2}\,\boldsymbol{s} : \boldsymbol{s}\right)^{1/2} / p_a$ is an effective stress ratio, $\eta_{pt}$ is a material parameter defining this ratio along the phase transformation (PT) line (Fig. 8), and $\xi^p$ is the cumulative plastic shear deformation ($\xi^p = \int_0^t \dot{\boldsymbol{\epsilon}}^p : \dot{\boldsymbol{\epsilon}}^p dt$, where t is time). Contraction or dilation is defined according to the $\eta$ value relative to $\eta_{pt}$. When $\eta < \eta_{pt}$ the stress point lies below the PT line and the soil behaves following a rule for contraction, and when $\eta > \eta_{pt}$ the stress point lies above the PT line and the soil behaves according to a rule for dilation. For the particular case when $\eta = \eta_{pt}$ the soil behavior will be controlled by the loading process. The function $\chi$ will be defined according to the scenarios discussed below.

#### 3.3.1 *Contraction zone*

$P''$ is given by:

$$3P'' = \chi(\eta, \eta_{pt}, p, a) = \zeta_\eta\, \psi_c \qquad (13)$$

The function $\zeta_\eta$ defines the rate of contraction according to Prevost [24]:

$$\zeta_\eta = \frac{(\eta/\bar{\eta})^2 - 1}{(\eta/\bar{\eta})^2 + 1} \qquad (14)$$

The function $\psi_c$ is newly introduced (Parra [23]) to scale the amount of contraction according to the level of confining pressure.

#### 3.3.2 *At and above phase transformation (PT) surface (Parra [23])*

As might be inferred from Figs. 1 - 5, above the PT line, tendency for dilation appears only during *loading* towards the failure surface, Upon load reversal or *unloading*, contraction takes over. In fact, Fig. 1 shows:

1. Dilation occurs during shear loading or increase of shear stress. During this phase, the rate of dilation is seen to increase with the increase of shear stress.

2. Contraction, upon load reversal or *unloading*, develops almost instantaneously, and the stress path in the $p - q$ plot moves toward the point where dilation started . In other words, contraction appears to depend on the amount of dilation experienced by the soil structure.

3. In the loading cycles close to the condition $p = 0$ (Fig. 1), it may be observed that a large change in shear strain occurs with minimal change in shear stress in the vicinity of phase transformation, from contractive to dilative response. Consequently, it was decided to directly model the accumulated strain as an additional response phase between contraction and dilation. If the PT line is reached during contraction and loading continues, additional stress increments are treated with the condition $P'' = 0$ until a user specified shear strain is accumulated. Thereafter, the dilative phase starts as described above.

4. In situations where a so called "driving stress" is present (*e.g.,* triaxial test with initial stress bias as shown in Fig. 2), a finite increment of accumulated permanent strain is incurred for each cycle of load (at $p \rightarrow 0$). The model includes a special scheme to account for that(Parra [23]).

### 3.4 *Hardening Rule (Parra [23])*

All surfaces, but the outermost ( [19, 22, 24]), may be translated in stress space without changing in form (in any deviatoric plane) and with no intersection. Therefore, the direction of translation $\boldsymbol{\mu}$ of the active yield surface $f_m$ was defined by a new relationship (Parra [23]) such that no overlap or intersection is allowed between the yield surfaces. The outermost surface remains stationary at all times.

### 3.5 *Model Performance*

Figures 5 and 9 show the performance and versatility of the developed model. Figure 9 may be compared to Figure 2, and depicts the important element of tracking the cycle-by-cycle accumulation of shear deformations.

## 4. FINITE ELEMENT FORMULATION

Soil is modeled as a two phase material using the Biot [3] formulation of porous media. This formulation is incorporated in a general purpose 2-D finite element program (Ragheb [25], Parra [23]) using the u - p approach (in which displacement of the soil skeleton, u, and pore pressures, p, are the unknowns) as suggested by Zienkiewicz *et al.* [33]. The computational scheme follows the methodology of Chan [7], which is based on the following assumptions: small deformations and rotations, density of the solid and fluid is constant in both time

and space, porosity is locally homogeneous and constant with time, soil grains are incompressible, and accelerations are equal for the solid and fluid phases. Therefore, the general coupled formulation after the spatial discretization and Galerkin approximation is expressed as follows:

$$\mathbf{M}\ddot{\mathbf{u}} + \int_{\Omega} \mathbf{B}^T \boldsymbol{\sigma}' \, d\Omega - \mathbf{Q}\,\bar{\mathbf{p}} - \mathbf{f}^S = \underline{0} \quad (15)$$

$$\mathbf{G}\ddot{\mathbf{u}} + \mathbf{Q}^T\,\dot{\mathbf{u}} + \mathbf{H}\,\bar{\mathbf{p}} + \mathbf{S}\,\dot{\bar{\mathbf{p}}} - \mathbf{f}^p = \underline{0} \quad (16)$$

where $\mathbf{M}$ is the mass matrix, $\mathbf{B}$ is the strain-displacement matrix, $\boldsymbol{\sigma}'$ is the effective stress vector, $\mathbf{Q}$ is the discrete gradient operator coupling the solid and fluid phases, $\bar{\mathbf{u}}$ is the displacement vector, $\bar{\mathbf{p}}$ is the pore pressure vector, $\mathbf{G}$ is the dynamic seepage force matrix, $\mathbf{H}$ is the permeability matrix, $\mathbf{S}$ is the compressibility matrix, and $\mathbf{f}^S$ and $\mathbf{f}^p$ are the prescribed boundary conditions for solid and fluid phase respectively. A superposed dot denotes time derivative. Viscous damping may be added for the solid phase in the form of Rayleigh damping ($\mathbf{C} = \alpha\mathbf{M} + \beta\mathbf{K}$, where $\mathbf{K}$ is the initial stiffness matrix). For earthquake loading problems, $\mathbf{G}$ is usually neglected so that symmetry of the global matrix is attained.

Eq. 15 and 16 are integrated in time using a simple single step predictor multi-corrector scheme of the Newmark type (Katona and Zienkiewicz [20]), with an automatic time stepping split algorithm, incorporated to improve the rate of convergence. The predictor is calculated using the initial stiffness matrix method (Zienkiewicz [34]), as the high degree of non-associativity (in the behavior of the solid phase) produces a non-symmetric tangent stiffness matrix that requires a non-symmetric matrix solver. Experience based on analyses of non-associative plasticity shows that the initial stiffness method performs reasonably well (Chan [7], Van Langen and Vermeer [30]). The second term in Eq. 15 is defined by the soil constitutive model as described above (Parra [23]).

The finite-element and constitutive-model package was calibrated and employed to conduct a large number of computations (Parra [23]) based on recorded centrifuge experimental response. The computation included one-dimensional site response with and without lateral spreading, and response of embankments on liquefiable soils. Remediation efforts by sand densification under the embankment toes were also analyzed (Parra [23]).

Figure 10 depicts a comparison between recorded and computed ground motion for the Port Island site. In this case history, the necessary model parameters were obtained through a simple system identification technique based on the recorded downhole accelerations (Elgamal [12]).

## 5. SUMMARY AND CONCLUSIONS

A new constitutive model is developed to model cyclic shear behavior during liquefaction. The underlying mechanisms are based on observed soil response during earthquakes, centrifuge experiments and cyclic laboratory tests. In this paper, the analytical and computational framework behind this model was presented. In addition the salient model response characteristics were illustrated.

## 6. ACKNOWLEDGMENTS

The research reported herein was supported by the Pacific Earthquake Engineering Research Center (PEER), the United States Geological Survey (grant No. 1434-HQ-97-GR-03070), INTEVEP, SA, Venezuela, and the National Science Foun-

dation (grant No. MSS-9057388). This support is gratefully acknowledged. The employed Port Island downhole acceleration data were provided by the Committee of Earthquake Observation and Research in the Kansai Area (CEORKA), Japan, with the help of Dr. Y. Iwasaki.

# References

[1] Arulmoli, K., Muraleetharan, K. K., Hossain, M. M. and Fruth, L. S. (1992). "VELACS: VELACS: Verification of Liquefaction Analysis by Centrifuge Studies, Laboratory Testing Program, Soil Data Report", *The Earth Technology Corporation, Project No. 90-0562*, Irvine, California.

[2] Baker, R. and Desai, C. S. (1982). "Consequences of Deviatoric Normality in Plasticity with Isotropic Strain Hardening," *International Journal for Numerical and Analytical Methods in Geomechanics*, Vol. 6, pp. 383 – 390.

[3] Biot, M. A. (1962). "The Mechanics of Deformation and Acoustic Propagation in Porous Media", *J. Appl. Phys.*, Vol. 33, No. 4, 1482–1498.

[4] Casagrande, A. (1975). "Liquefaction and Cyclic Deformation of Sands - A critical Review," Proceedings, 5th Pan-American Conference on Soil Mechanics and Foundation Engineering, Buenos Aires, Argentina; also published as Harvard Soil Mechanics Series No. 88, January 1976, Cambridge, Mass.

[5] Castro, G. (1975). Liquefaction and Cyclic Mobility of Saturated Sands. Journal of the Geotechnical Engineering Division, ASCE, 101, GT6, 551-569.

[6] Castro, G and Poulos, S. J. (1977). "Factors Affecting Liquefaction and Cyclic Mobility," Journal of the Geotechnical Engineering Division, ASCE, Vol. 103, No. GT6, June, pp. 501-516.

[7] Chan, A. H. C. (1988). "A Unified Finite Element Solution to Static and Dynamic Problems in Geomechanics", *Ph.D. dissertation*, University College of Swansea, U. K.

[8] Desai, C. S. and Siriwardane H. J. (1984). *Constitutive Laws for Engineering Materials - With Emphasis on Geologic Materials*, Prentice-Hall Inc., New Jersey.

[9] Dobry, R., Taboada, V. and Liu, L. (1995). "Centrifuge Modeling of Liquefaction Effects During Earthquakes," Proc. 1st Intl. Conf. On Earthquake Geotechnical Engineering (IS-Tokyo), Keynote Lecture, Ishihara, K. Ed., 3, Balkema, Nov. 14-16, Tokyo, Japan, 1291-1324.

[10] Dobry, R. and Abdoun, T. (1998). "Post-Triggering Response of Liquefied Sand in the Free Field and Near Foundations", Proc. Geot. Eq. Engrg. and Soil Dynamics III, V1, Dakoulas, P., Yegian, M. and Holtz., R. D., Eds., Geot. Special Publication No. 75, ASCE, Seattle, Washington, Aug 3-6, keynote lecture, 270-300.

[11] Elgamal, A. -W., Zeghal, M., and Parra, E. (1995). "Identification and Modeling of Earthquake Ground Response," Proc. 1st

Intl. Conf. On Earthquake Geotechnical Engineering (IS-Tokyo), Special, Keynote and Theme Lectures Volume, Nov. 14-16, Tokyo, Japan.

[12] Elgamal, A. -W., Zeghal, M., and Parra, E. (1996a). "Liquefaction of Reclaimed Island in Kobe, Japan," J. Geotech. Engineering, ASCE, 122, 1, Jan., 39-49.

[13] Elgamal, A. -W., Zeghal, M., Taboada, V. M. and Dobry, R. (1996b). "Analysis of Site Liquefaction and Lateral Spreading using Centrifuge Model Tests," Soils and Foundations, 36, 2, June, 111-121.

[14] Elgamal, A. -W., Dobry, R., Parra, E. and Yang, Z. (1998) *Soil Dilation and Shear Deformations During Liquefaction*, Proc. 4th Intl. Conf. on Case Histories in Geotechnical Engineering, S. Prakash, Ed., St. Louis, MO, March 8-15, 1998.

[15] Hill, R. (1950) *The Mathematical Theory of Plasticity*, Oxford Univeristy Press, London.

[16] Holzer, T. L., Youd T. L. and Hanks T. C. (1989). "Dynamics Of Liquefaction During the 1987 Superstition Hills, California, Earthquake," Science, Vol. 244, 56-59.

[17] Iai, S. (1991). "A Strain Space Multiple Mechanism Model for Cyclic Behavior of Sand and its Application," Earthquake Engineering Research Note No. 43, Port and Harbor Research Institute, Ministry of Transport, Japan.

[18] Iai, S., Morita, T., Kameoka, T., Matsunaga, Y. and Abiko, K. (1995). "Response of a Dense Sand Deposit During 1993 Kushiro-Oki Earthquake," Soils and Foundations, 35, 1, March, 115-131.

[19] Iwan, W. D. (1967) "On a class of Models for the Yielding Behavior of Continuous and Composite Systems," *Journal of Applied Mechanics, ASME*, Vol. 34, pp. 612 – 617.

[20] Katona, M. G. and Zienkiewicz, O. C. (1985). "A Unified Set of Single Step Algorithms. Part 3: The Beta-m Method, A Generalization of the Newmark Scheme", *Int. J. Num. Meth. Engrg.*, Vol. 21, 1345–1359.

[21] Lacy, S. (1986) "Numerical Procedures for Nonlinear Transient Analysis of Two-phase Soil System," *Ph.D. dissertation*, Princeton University, NJ, U.S.A.

[22] Mroz, Z. (1967) "On the Description of Anisotropic Work Hardening," *Journal of the Mechanics and Physics of Solids*, Vol. 15, pp. 163 – 175.

[23] Parra, E. (1996). "Numerical Modeling of Liquefaction and Lateral Ground Deformation including Cyclic Mobility and Dilative Behavior in Soil Systems", *Ph.D. dissertation*, Dept. of Civil Engineering, Rensselaer Polytechnic Institute, in progress.

[24] Prevost, J. H., (1985) "A Simple Plasticity Theory for Frictional Cohesionless Soils," *Soil Dynamics and Earthquake Engineering*, Vol. 4, No. 1, pp. 9 – 17.

[25] Ragheb, A. (1994). Numerical analysis of Seismically Induced Deformations in Saturated Granular Soil Strata. *Ph.D. Thesis*, Rensselaer Polytechnic Institute, Troy, NY.

[26] Seed, H. B. and Lee, K. L. (1966). "Liquefaction of Saturated Sands During Cyclic Loading," Journal of the Soil Mechanics and Foundations Division, ASCE, 92, SM6, Nov., 105–134.

[27] Seed, H. B. (1979). "Soil Liquefaction and Cyclic Mobility Evaluation for Level Ground During Earthquakes," J of the Geotech Engng Div, ASCE, 105, No. GT2, Feb., 201-255.

[28] Taboada, V. M. (1995) Centrifuge Modeling of Earthquake-Induced Lateral Spreading in Sand using a Laminar Box *Ph.D. Thesis*, Rensselaer Polytechnic Institute, Troy, NY.

[29] Tateishi, A., Taguchi, Y, Oka, F. and Yashima, A. (1995). "A Cyclic Elasto-Plastic Model For Sand and Its Application Under various Stress Conditions," Proc. 1st Intl. Conf. On Earthquake Geotech Engng, 1, 399-404, Balkema, Rotterdam.

[30] Van Langen, H. and Vermeer, P. A. (1990). "Automatic Step Size Correction for Non-associated Plasticity Problems", *Int. J. Num. Meth. Engrg.*, Vol. 29, 579–598.

[31] Youd, T. L., and Holzer, T. L. (1994). "Piezometer Performance at the Wildlife Liquefaction Site." *J. Geotech. Engrg.*, ASCE, 120(6), 975-995.

[32] Zeghal, M. and Elgamal, A. -W. (1994). "Analysis of Site Liquefaction Using Earthquake Records," Journal of Geotechnical Engineering, ASCE, 120, No. 6, 996-1017.

[33] Zienkiewicz, O. C., Chan, A. H. C., Pastor, M., Paul, D. K., and Shiomi, T. (1990). "Static and Dynamic Behaviour of Soils: A Rational Approach to Quantitative Solutions: I. Fully Saturated Problems," *Proc. R. Soc. Lond.*, A 429, 285–309.

[34] Zienkiewicz, O. C. (1991). *The Finite Element Method*, Vol. 2, *Solid and Fluid Mechanics Dynamics and Non-Linearity,* $4^{th}$ Ed., McGraw Hill, London.

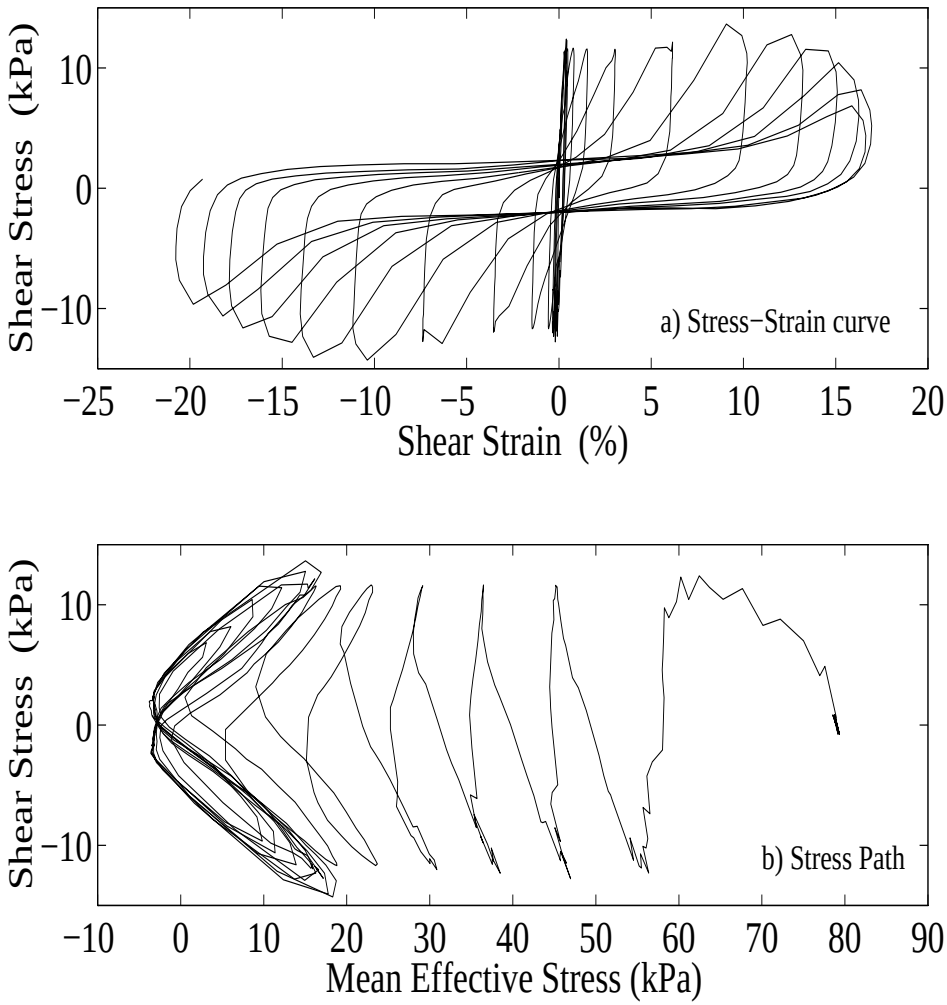


**Figure 1: Stress-strain curve and stress path for Nevada Sand with $D_r = 60\%$ obtained from undrained cyclic simple shear (CSS) test (Arulmoli et al., 1992).**

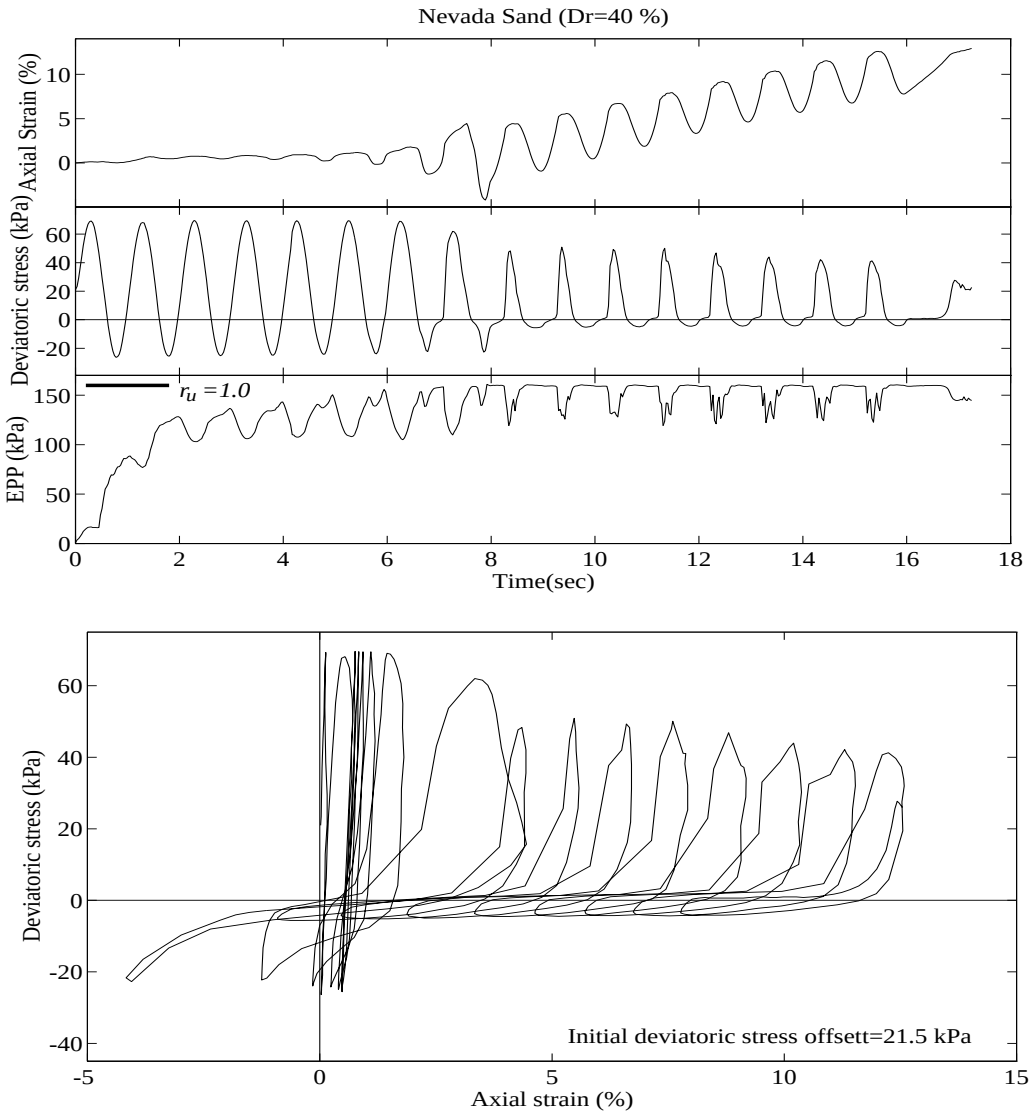


Figure 2: Stress, strain and EPP histories during an undrained stress-controlled cyclic triaxial test of Nevada sand ($Dr = 40$ %) with an imposed static (initial) deviatoric stress (after Arulmoli et al. 1992).

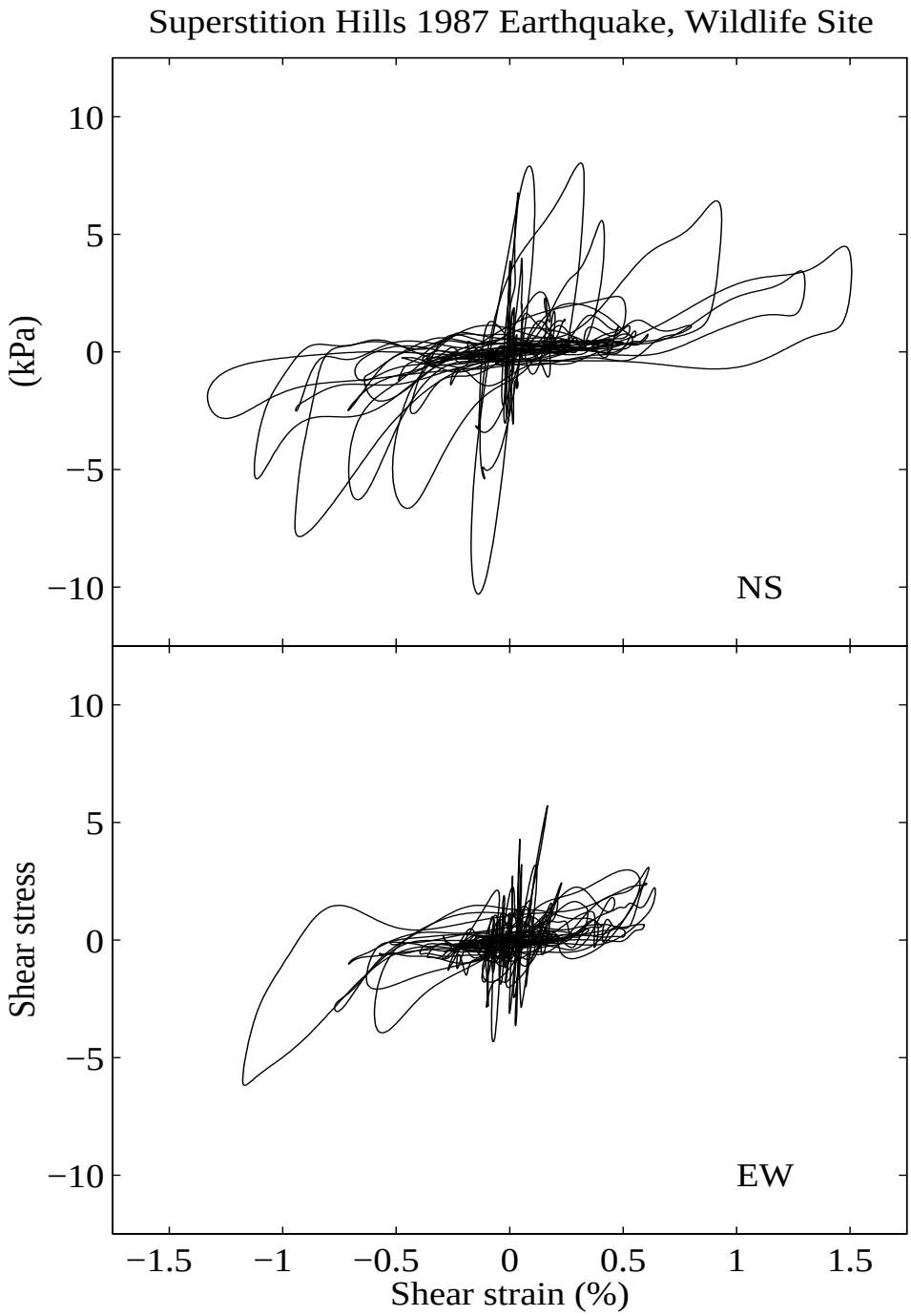


Figure 3: Wildlife-Refuge NS and EW shear stress-strain histories during the Superstition Hills 1987 Earthquake ( Zeghal and Elgamal 1994 ).

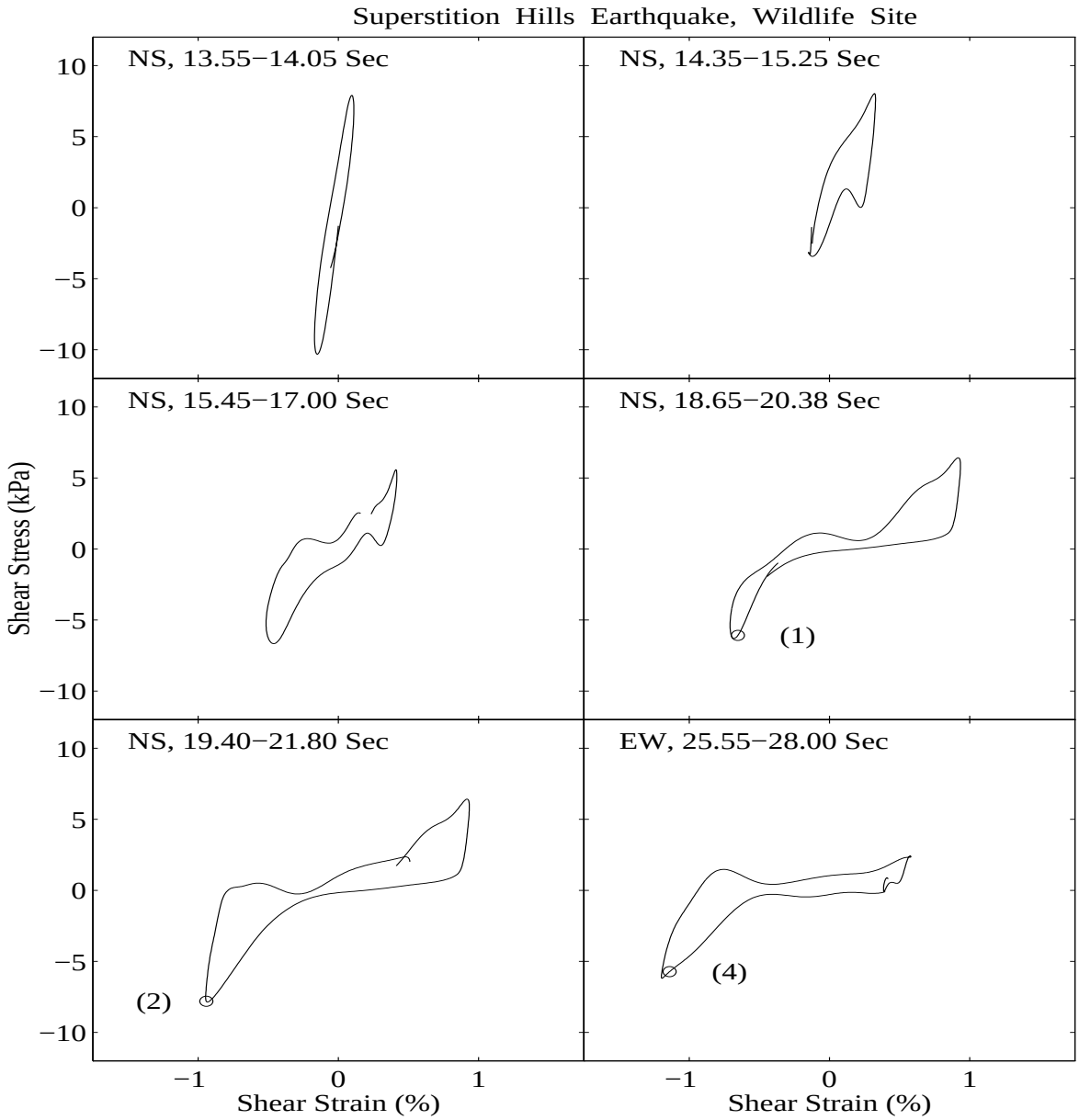


Figure 4: Shear stress-strain history during selected loading cycles of the Superstition Hills earthquake ( Zeghal and Elgamal 1994 ).

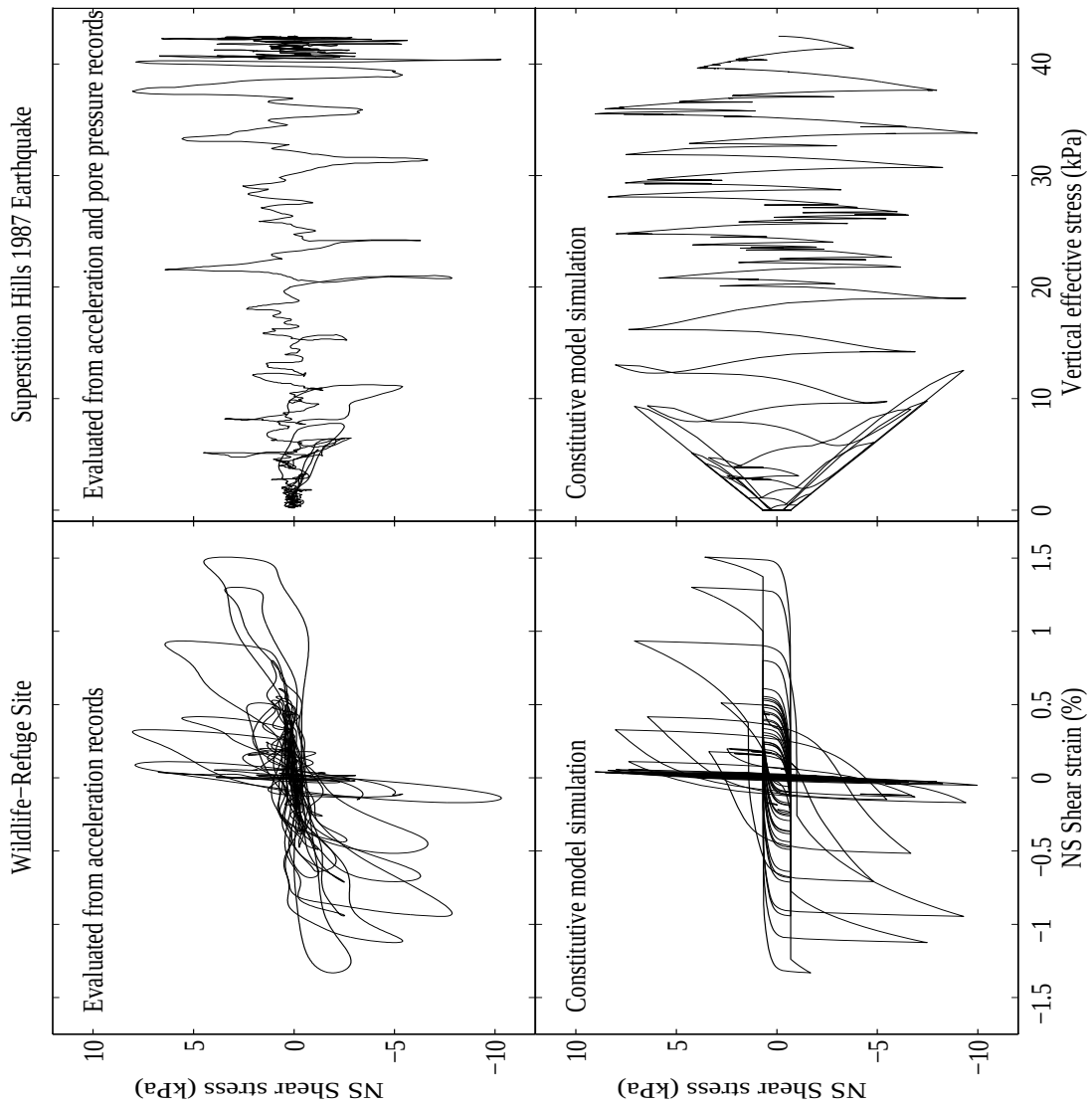


Figure 5: Wildlife-Refuge NS shear stress-strain and effective-stress histories during the Superstition Hills 1987 Earthquake (evaluated from acceleration histories and computed). (after Elgamal et al. 1995).

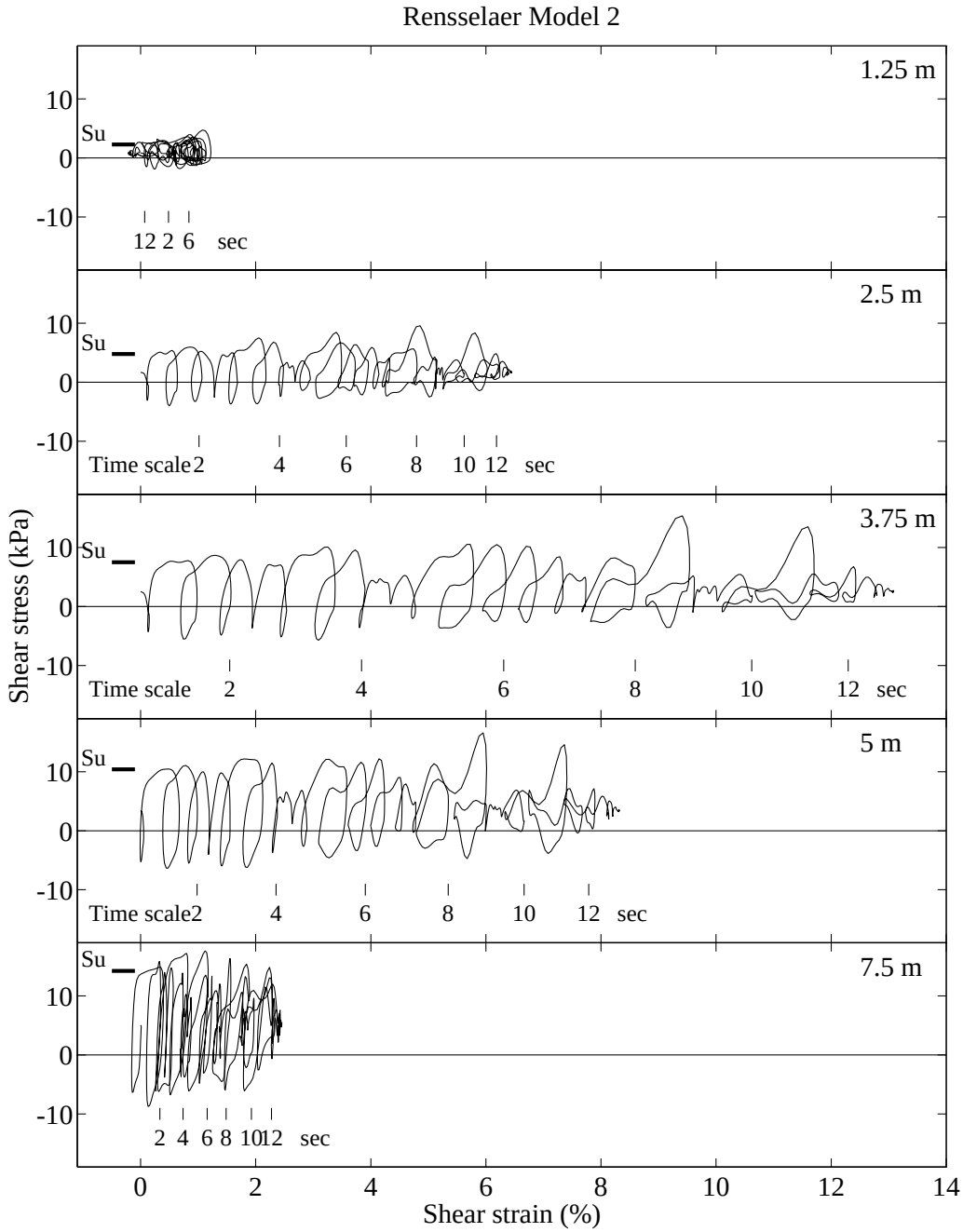


Figure 6: RPI Model 2 shear stress-strain histories with superposed static stress due to inclination (Taboada 1995, Dobry et al. 1995, Elgamal et al. 1996b).

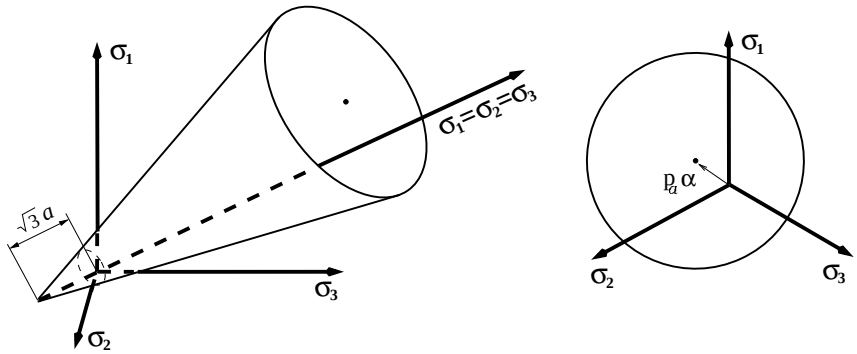


Effective principal stress space  Deviatoric or $\pi$ plane

**Figure 7: Conical yield surface in principal stress space and deviatoric or $\pi$ plane (Prevost 1985, Lacy 1986, Parra 1996).**

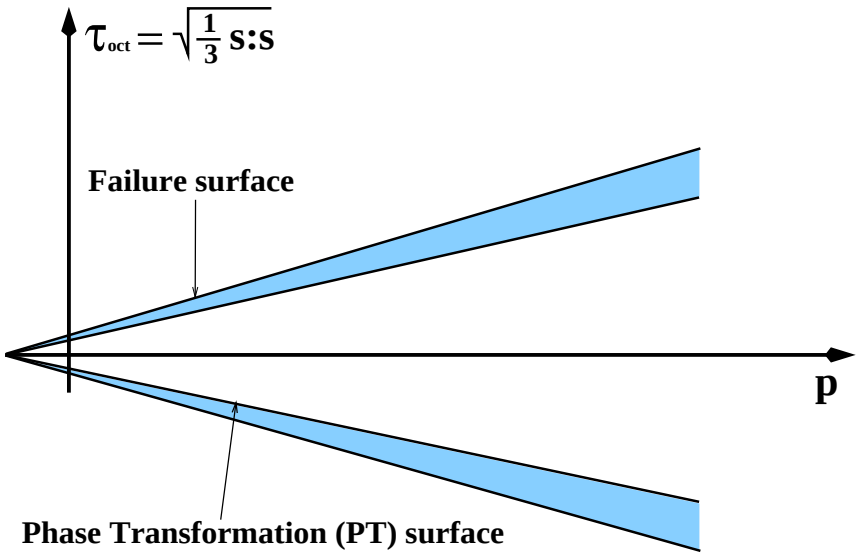


**Figure 8: Yield function and phase transformation line (Parra 1996).**

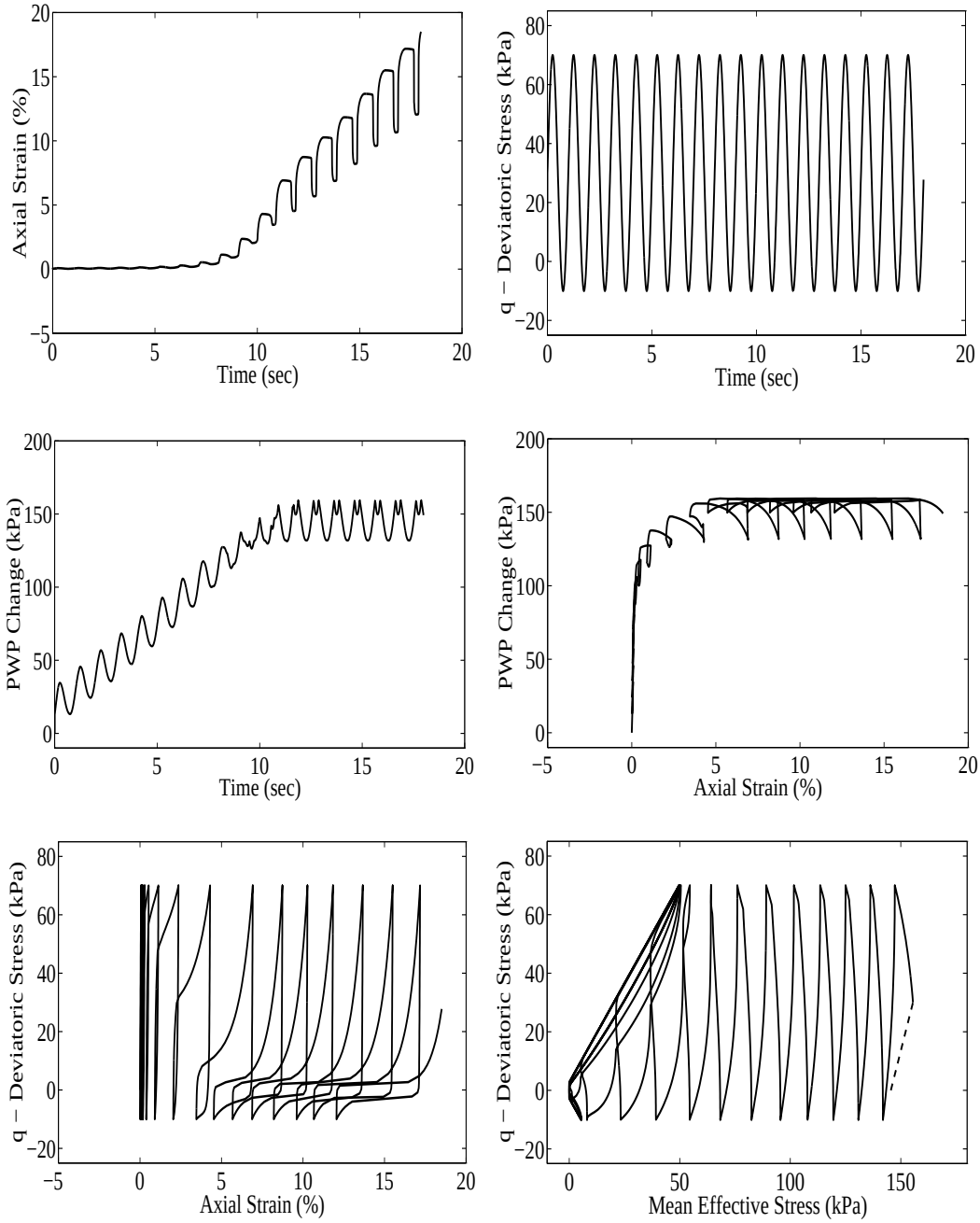


**Figure 9: Simulation of a cyclic triaxial undrained test with stress bias ($\mathrm{CIUC}_{cyclic}$), Parra (1996).**

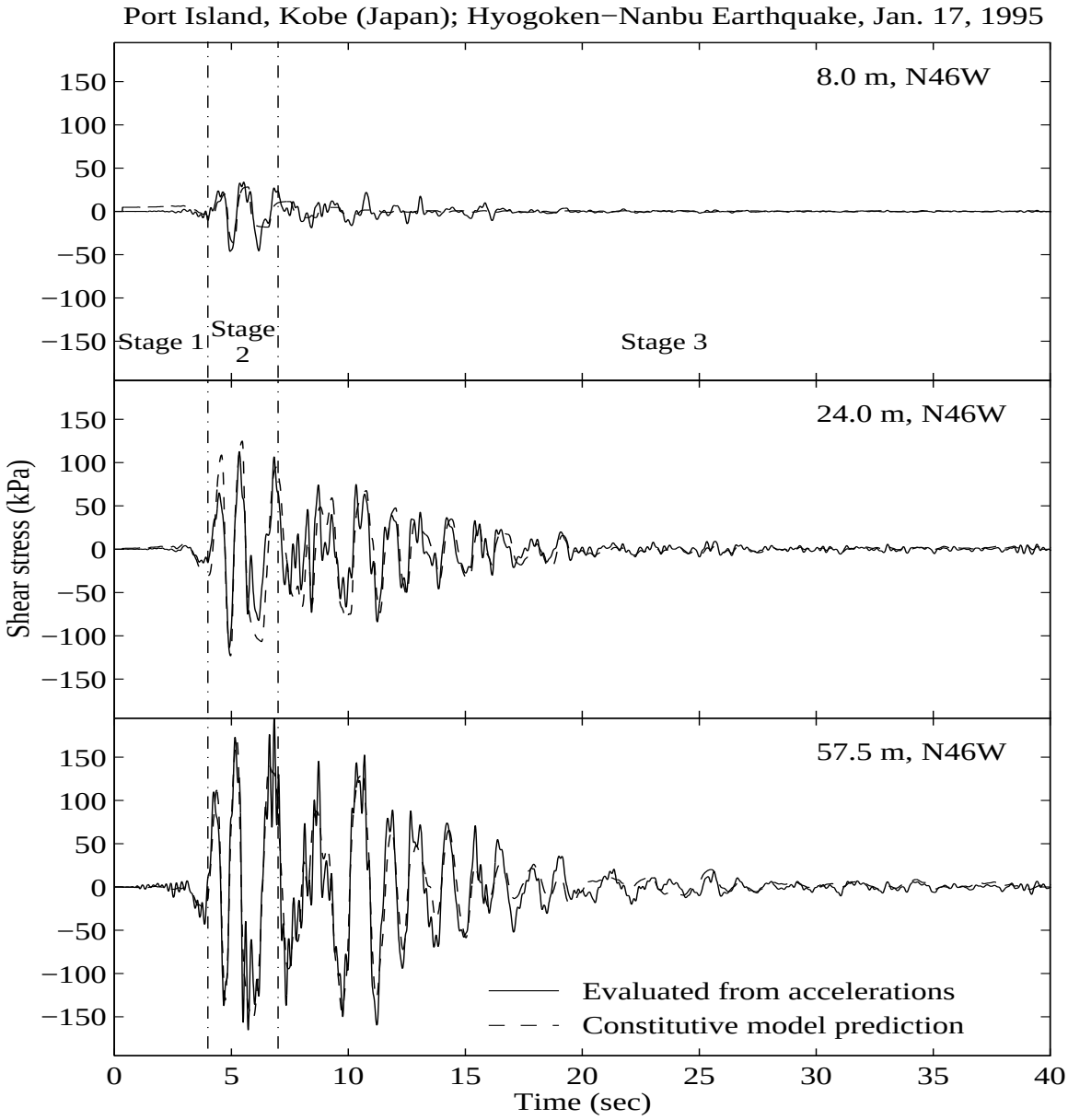


Figure 10: Port Island shear stress histories estimated from acceleration histories and corresponding constitutive model prediction (at 8.0 m, 24.0 m, and 57.5 m depths), after Elgamal et al. (1996a).